Volume 77, number 2,3 OPTICS COMMUNICATIONS 15 June 1990

Full length article

NONLINEAR MULTI TWO-WAVE MIXING, THE FANNING PROCESS AND ITS BLEACHING IN PHOTOREFRACTIVE MEDIA

Mordechai SEGEV, Yoav OPHIR and Baruch FISCHER
Department of Electrical Engineering, Technion–Israel Institute of Technology, Haifa 32000, Israel

Received 28 November 1989; revised manuscript received 12 February 1990

A theoretical and experimental study of photorefractive nonlinear multi two-wave mixing is given. It is used to describe the fanning effect, which is an asymmetric self induced light scattering process, and is shown to originate from amplified noise. The cross section of the input beam is found to be very influential on the fanning strength. We also describe the bleaching mechanism of the fanning when a signal beam is added and amplified by two-beam coupling.

We have recently reported [1] on various nonlinear mode coupling effects in photorefractive waveguides. In a funnel-like process, for example, the low order spatial modes of a slab waveguide were shown to be amplified at the expense of the high order modes. The opposite anti-funneling process with an amplification of the high order modes occurred for beam coupling with opposite sign. A similar mechanism provided a method for amplifying and launching a guided beam in a waveguide by a lateral pumping. The fanning effect [2–5] is another self scattering process in photorefractive media in which a single light beam self generates scattering in an asymmetrical way. This effect is known for about ten years. Its exact origin and theoretical description, however, are still not fully studied and understood. The question if it is caused by amplified noise [2] or by amplified spatial frequencies of the beam itself [3] is still open. The understanding requires the use of a basic analysis of multi two-wave mixing in thick photorefractive media.

In this paper we present an analysis of the asymmetric fanning effect in thick photorefractive crystals. We find that amplified noise plays an important role in producing the fanning effect. The size of the cross section in the crystal is another important parameter. A reduction of the spot size of the beam weakens the fanning. We also show that a small signal beam causes a bleaching (broad "hole burning") in the spatial frequency spectrum of the fanning in a similar way to the bleaching in the frequency dependent gain profile in atomic transitions. Such a comparison can lead us to view the fanning effects as a kind of amplified spontaneous emission in inverted atomic systems. The bleaching effect in the fanning is studied theoretically and experimentally. The motivation of the study originated from the mode coupling effects in waveguides, in which the mode coupling gave the funneling and anti-funneling processes. Our present objective is the general multi two-wave mixing process in photorefractive bulks. Elsewhere it will be shown that the coupling can also give self-focusing and defocusing effects.

The analysis is based on the guidelines and notations of our recent work [1]. We extend the photorefractive two-wave mixing equations to many waves with a two-wave mixing process for every pair i and j of N plane waves, each propagating in a different direction in a certain plane. The linear summation of these components is possible where the coupling of each pair is small (the small gratings modulation approximation), for which the two-wave mixing equations were developed. Then, the coupled wave equations are [1]

$$\frac{\mathrm{d}\tilde{I}_i}{\mathrm{d}z}=\frac{1}{I_0}\sum_{j\neq i}\Gamma_{ij}\tilde{I}_i\tilde{I}_j\,,\quad \frac{\mathrm{d}\phi_i}{\mathrm{d}z}=\frac{1}{I_0}\sum_{j\neq i}\Gamma'_{ij}\tilde{I}_j\,, \tag{1}$$

where $\tilde{I}_i+I_i\cos\alpha_i$, I_i and ϕ_i are the intensity and the added phase due to the coupling of beam i. [We note

that such redefinition of the beams' intensities permits using the known analytical solutions [6] of photorefractive four-wave mixing for beams with the same angles (with the crystal normal) for the general nonequal angles case.] $I_0 = \sum_{i=1}^{N} I_i$ and

$$\Gamma_{ij} = -\Gamma_{ji} = \left(\frac{1}{\cos\alpha_i \cos\alpha_j}\right) 2\,\mathrm{Re}\,\gamma_{ij}\,,$$

$$\Gamma'_{ij} = -\Gamma'_{ji} = \left(\frac{1}{\cos\alpha_i \cos\alpha_j}\right) \mathrm{Im}\,\gamma_{ij}\,. \qquad (2)$$

α_i are the angles with the z-direction (along the c-axis) as shown in fig. 1, γ_{ij} is the coupling parameter given by [1]

$$\gamma_{ij} = -\frac{i\omega}{2c}\frac{(r_{\mathrm{eff}})_{ij} n_o^3}{} E_m\,. \qquad (3)$$

$(r_{\mathrm{eff}})_{ij}$ and E_m are the effective electro-optic coefficient and an internal field which depend on the geometry (angles α_i and α_j) and the material parameters. For extraordinary polarizations in $BaTiO_3$,

$$(r_{\mathrm{eff}})_{ij} = \left(\frac{1}{n_o n_e^3}\right)\Big[n_e^4 r_{33} \sin\alpha_i \sin\alpha_j + 2 n_e^2 n_o^2 r_{42} \cos^2\left(\frac{\alpha_i+\alpha_j}{2}\right) + n_o^4 r_{13} \cos\alpha_i \cos\alpha_j \Big] \sin\left(\frac{\alpha_i+\alpha_j}{2}\right). \qquad (4)$$

r_{ij} are the electro-optic coefficients (in $BaTiO_3$ r_{42} is much larger than the others), n_o and n_e are the ordinary and extraordinary refractive indices and E_m is given by [6]

$$E_m = \frac{E_p(E_d - iE_0)}{E_0 + i(E_d + E_p)}(\hat{e}_i \cdot \hat{e}_j^*)\,, \qquad (5)$$

where $\hat{e}_i$ are unit vectors along the beam polarizations [for extraordinary polarization $(\hat{e}_i \cdot \hat{e}_j^*) = \cos(\alpha_i - \alpha_j)$]. E_0 is the applied electric field, $E_d = k_B T k_g / e$ and $E_p = e p_d / \epsilon k_g$, p_d is the density of traps, k_B is Boltzman's constant, T the temperature, e the electron charge, k_g the gratings' wavenumber given by $k_g = (4\pi n_e/\lambda)\sin[(\alpha_i - \alpha_j)/2]$ and λ is the wavelength in free space. ϵ is the dc permittivity along the gratings given by $\epsilon = \epsilon_0(\epsilon_c \cos^2\theta + \epsilon_a \sin^2\theta)$ where $\theta = 90^\circ - [(\alpha_i + \alpha_j)/2]$ is the angle between $\vec{k}_g$ and the c-axis and ϵ_c and ϵ_a are the parallel and perpendicular (to the c-axis) relative to the free space permittivity (ϵ_0). In our calculations below we have used the following $BaTiO_3$ crystal parameters [1]: $r_{42} = 1640 \times 10^{-12}$ V/m, (r_{33} and r_{13} are negligible compared to r_{42}), $\epsilon_a = 4300$, $\epsilon_c = 106$, $n_o = 2.488$, $n_e = 2.424$ and $p_d = 2 \times 10^{16}$ cm^{-3}.

A continuous version of eq. (1) can be obtained where the plane waves which propagate in slightly different directions in the yz-plane can be considered as the Fourier transform components of a general spatial optical field with spatial frequencies $q = (2\pi n_e/\lambda)\sin(\alpha - \alpha_0)$, where α_0 is the mean propagation angle with the z-axis. Then eq. (1) becomes

$$\frac{d\tilde{F}(q)}{dz} = \frac{1}{F_0}\int_{-\infty}^{\infty} \Gamma(q, q')\,\tilde{F}(q)\,\tilde{F}(q')\,dq'\,,$$

$$\frac{d\phi(q)}{dz} = \frac{1}{F_0}\int_{-\infty}^{\infty} \Gamma'(q, q')\,\tilde{F}(q')\,dq'\,, \qquad (6)$$

where

$$\tilde{F}(q) = F(q)\cos\alpha\,,$$

$$F(q) = \left|\int_{-\infty}^{\infty} A(y)\exp(-iqy)\,dy\right|^2\,,$$

$$F_0 = \int_{-\infty}^{\infty} F(q)\,dq = 2\pi\int_{-\infty}^{\infty} |A(y)|^2\,dy\,,$$

(Parseval's identity), and $A(y)$ is the beam amplitude which is dependent on the transversal y-direc-

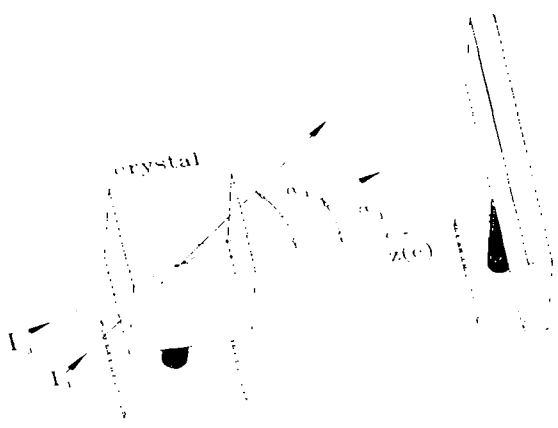

Fig. 1. The crystal and the beams in a multi wave mixing geometry.

tion. The use of only one dimensional q is possible since the coupling in $BaTiO_3$ is very strong in the polarization direction, which is along the y-direction (in fact, in the yz-plane) and not significant in the x-direction. Therefore, we have integrated the light intensities in the x-direction in our experiments and calculations which are reported in this paper. It is possible however, to extend the analysis to spatial frequencies in two dimensions. Then $q \rightarrow \bar{q} = (q_x, q_y)$, and $\tilde{F}$ and Γ are functions of $(\bar{q})$. For simplicity, this was not done in the present paper. Eq. (6) gives the z-dependence of $\tilde{F}(q)$ due to the photorefractive coupling. It gives, for example, the description of a pictorial field as it propagates in the crystal where the photorefractive interaction evokes a coupling between the spatial frequency components (in the y-direction). The specific case of a gaussian beam input is a simple example for applying this method.

Eq. (1) can be solved analytically for each isolated pair of interacting beams $\tilde{I}_i$ and $\tilde{I}_j$ with given inputs $\tilde{I}_i(0)$ and $\tilde{I}_j(0)$ at $z=0$, where the other beams contribute only to the background. Then $\tilde{I}_i + \tilde{I}_j = \tilde{I}_i(0) + \tilde{I}_j(0)$ and

$$\tilde{I}_i(z) = \frac{\tilde{I}_i + \tilde{I}_j}{1 + [\tilde{I}_j(0)/\tilde{I}_i(0)] \exp(\tilde{\Gamma}_{ij} z)},$$

$$\tilde{I}_j(z) = \frac{\tilde{I}_i + \tilde{I}_j}{1 + [\tilde{I}_i(0)/\tilde{I}_j(0)] \exp(-\tilde{\Gamma}_{ij} z)}, \qquad (7)$$

with a renormalized coupling constant $\tilde{\Gamma}_{ij} = \Gamma_{ij}(\tilde{I}_i + \tilde{I}_j)/I_0$, due to the background intensity I_0 of all modes. This reduction of the effective coupling of each pair ensures the validity of the small gratings modulation approximation, for which the two-wave mixing equations were developed.

For the solution of the many interacting beams problem of eqs. (1) and (4), we have used two numerical approaches. In the first one, we divided the interaction length to small intervals and found by eq. (7) new intensities for every pair, assuming fixed initial values for all beams in each interval. We also used a given computer program for nonlinear coupled equations. Both ways gave the same results. We have also divided the spatial frequency range to small intervals, each representing a plane wave component. Then eq. (6) was used to obtain the nonlinear interaction effect in the frequency space. The output beam in the real space is the inverse transform, which gives the transversal y-dependence of the field.

Now we turn to the fanning effect. The first systematic report on asymmetric self-scattering was given by Voronov et al. [2] who used cerium doped strontium barium niobate (SBN) crystals. They suggested that the effect is caused by amplified noise. Feinberg reported [3] on the fanning effect in $BaTiO_3$ crystals. He suggested that the nonuniform intensity profile of the input beam induces (photorefractively) a nonuniform change of the refractive index. This is turn scatters the beam asymmetrically. His analysis of the effect is limited to a "thin" photorefractive medium (or short interaction lengths), and also neglects the gratings components which are not in the beams transversal plane. The fanning effect, however, must be treated with all gratings components in the "thick" and long interaction regime to account for beam depletion and the huge amplification of the scattered light. Since the two above explanations of the fanning effect can be possible mechanisms, the experimental description requires an exact analysis. Eqs. (1) and (6) with the interacting plane wave components provide a natural basis for such a calculation. Our conclusion below shows that in order to explain the fanning effect it is necessary to add noise to the system as the suggestion in ref. [2]. Therefore, we discuss in the next paragraph the way we added the noise into our equations.

The noise can be generated by scattering from surface roughness, from distributed defects and inhomogeneities in the crystal or from fluctuations of the space charge fields and the photofractively induced index changes. Assuming a type of Rayleight scattering can give us some quantitative feeling on the intensity and the angular dependence of the noise. It turns out that a $\cos^2(\alpha - \alpha_0)$ dependence of the intensity in Rayleight scattering (for parallel to the beams plane or extraordinary polarizations) gives a good description of the experiments (α_0 and α are the angles of the incident beam and a scattering component directions with the z-axis).

There is another geometrical factor in the coupling process with noise. It was found [5] that the fanning strength is strongly dependent on the location of the crystal in the path of a focused incident beam. The fanning was almost diminished where the dimension of the beam cross section was low. It was attributed to limited interaction with the noise components. It

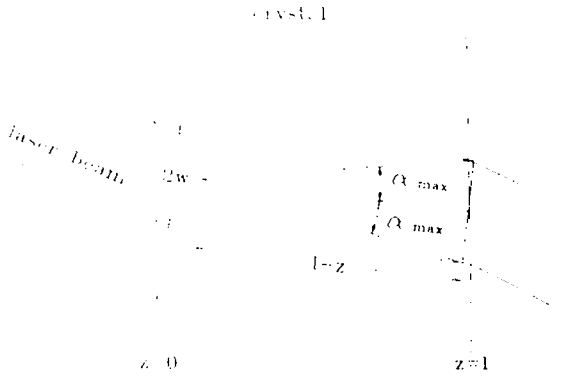

Fig. 2. A scheme of the beam in the crystal upon which the calculation of the angular width of the noise was based.

gives another angular dependent term for the noise amplification. We approximated this factor by taking into account only the noise in a window around α_0. The width of the window was chosen to be dependent on the beam diameter and the z-axis according to the angle of the diagonal from z to the output plane of the photorefractive crystal (see fig. 2). This gives a distributed input noise with increasing angular width as the beam propagates in the crystal, according to $\tan^{-1}[w/2(l-z)]$, where $w/2$ and l are the average spot size of the beam and the beam's length in the photorefractive crystal. (In fig. 2, $\bar{w}=w/2$ represents the a reduced spot size which is an average for the integration of the light intensities in the x-direction.) Thus, the overall distributed input noise that we inserted into eq. (6) is given by

$$\tilde{F}_{\text{noise}}(\alpha,z)=a\tilde{F}(q=0,\ z=0)\cos^2(\alpha-\alpha_0)\ ,$$
$$\text{for } |(\alpha-\alpha_0)| \leqslant \tan^{-1}[w/2(l-z)]\ ,$$
$$=0\ , \qquad \text{otherwise}\ . \tag{8}$$

The calculations below show that a noise intensity ratio with respect to the input beam's zero frequency of $a\approx 10^{-4}$ is needed to explain the experimental results. Other similar angular dependences of the noise, however, can give good qualitative results.

To understand the fanning effect we have presented side by side typical computational and experimental results as shown in figs. 3–6. In the experiment we used a poled $BaTiO_3$ crystal with dimensions of $5\times5\times5$ mm^3. The input beam was a gaussian beam with an extra-ordinary polarization which was loosely focused and had a propagation direction of 20° and 14.8° (inside the crystal) with the c-axis (z-direction). The power of the input beam was 10 mW and its waist about 12 μm. The experimental far field of the output beam (recorded by a video camera) is shown in fig. 3a for three values of the input beam average spot sizes: 0.1, 0.5 and 1 mm (by putting the crystal at different locations along the focused beam path).

In the analysis, we used the crystal parameters for the coupling constants from ref. [1]. According to the experiments, the calculation was performed for two angles of propagation for the gaussian input beam: 20° and 14.8° with respect to the c-axis. The distance along the z-axis in the crystal was 0.5 cm. We have decomposed the input gaussian beam into its spatial frequency Fourier components [$F(q)$] in the y-direction and applied our numerical method. The calculation was carried out with and without noise as described below. As mentioned above, it was found out that we needed a weak noise intensity ratio of $a\approx 10^{-4}$ to describe the fanning. Fig. 3b shows the calculated outputs in the frequency space (correspond to the output far field) for a beam propagation at 20° with the c-axis and for four values of the beam's spot size: 0.1, 0.5, 0.8 and 1 mm. Fig. 4, repeats fig. 3 for an angle of 14.8° and beam spot sizes of 0.1, 0.5 and 1 mm.

From figs. 3,4 we can see the agreement between the theoretical calculations and the experimental results. For these cases the noise was responsible for the developing of the left lobes. There is, however, an additional effect of the input beam self interaction (of its frequency components), which can be seen by comparing the input and the output. It can be clearly observable in cases where the fanning is low with very narrow beams and for low angles of beam propagation. Fig. 5 shows this effect on the main beam, which is nonuniformly depleted and shifted with respect to the input beam. The experiment and the calculation (figs. 5a and 5b, respectively) show a shift of about 0.2° towards the c-axis from the main beam direction with a small change of the shape. The propagation angle was 12.5° with the c-axis and the waist of the beam was 15 μm inside the crystal. Another specific example of beam propagation along the $\pm c$ axis ($\alpha_0=0$, 180°) gives symmetric self defocusing and focusing effects [1,7].

It is important to note that we have neglected in

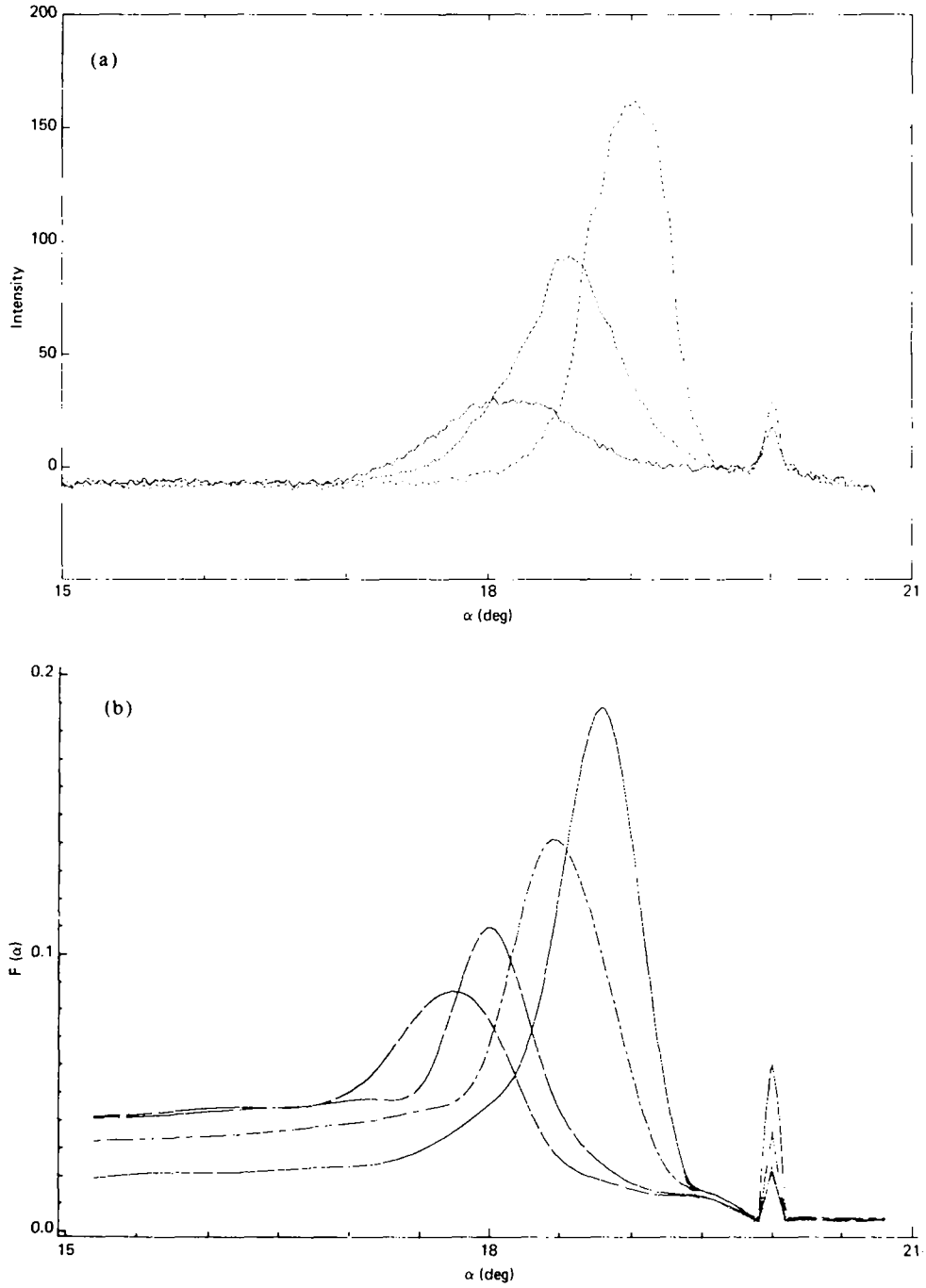

Fig. 3. (a) Experimental and (b) theoretical outputs showing the asymmetric self scattering for a gaussian input beam that propagates (from $z=0$ to $z=0.5$ cm) at an angle of 20° with the c-axis for three average spot sizes of the input beam: 0.1, 0.5 and 1 mm. In (b) another curve for 0.8 is given. The curves which are more smeared to the left corresponds to higher spot sizes. The figure shows the spatial frequencies dependence or the output's far field. All angles are taken inside the crystal and the intensities are given in arbitrary units.

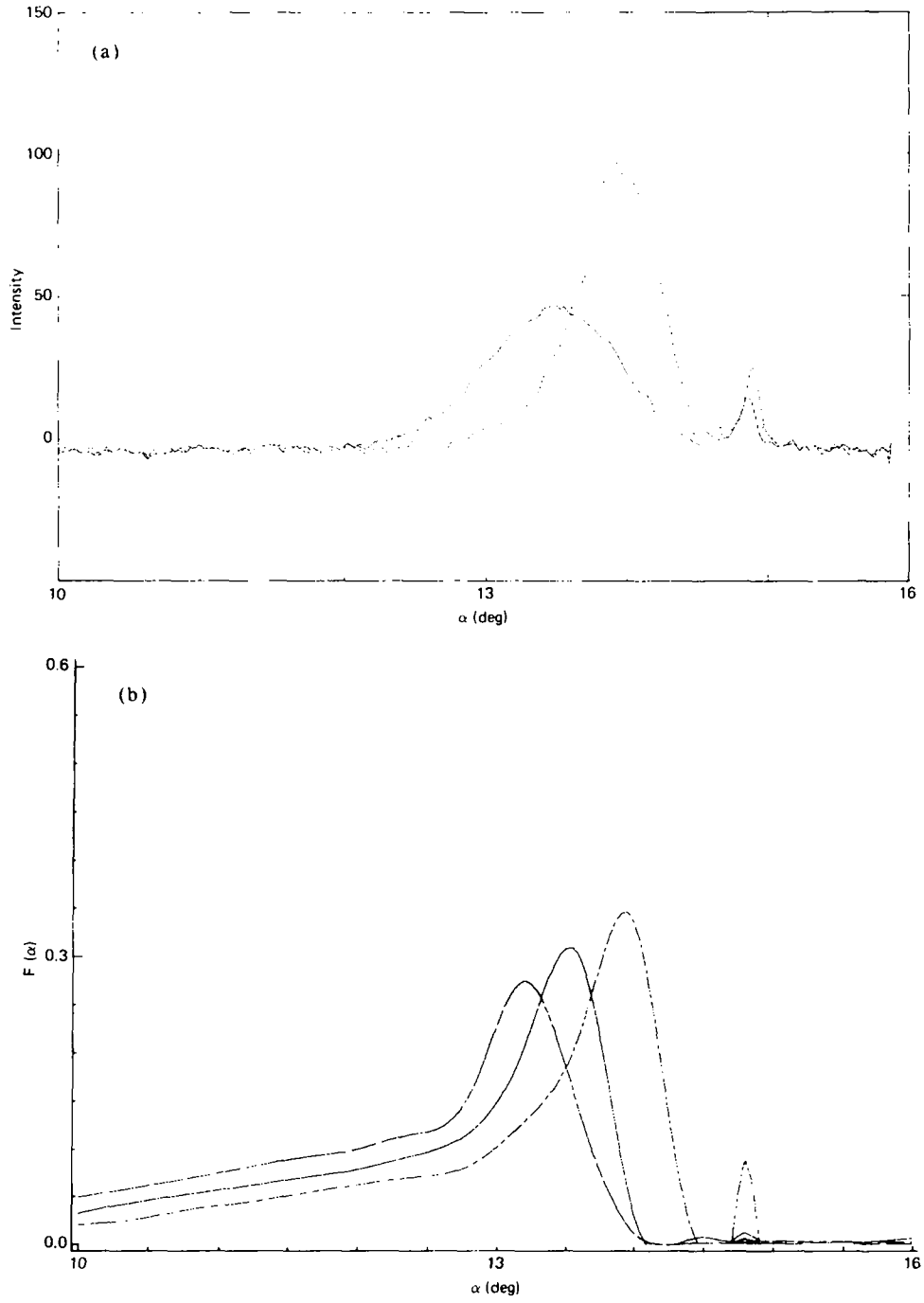

Fig. 4. As in fig. 3, (a) experimental and (b0 theoretical output showing the fanning, for a gaussian input beam that propagates (from $z=0$ to $z=0.5$ cm) at an angle of 14.8° with the c-axis for three average spot sizes of the input beam: 0.1, 0.5 and 1 mm. The curves which are more smeared to the left corresponds to higher spot sizes. All angles are taken inside the crystal and the intensities are given in arbitrary units.

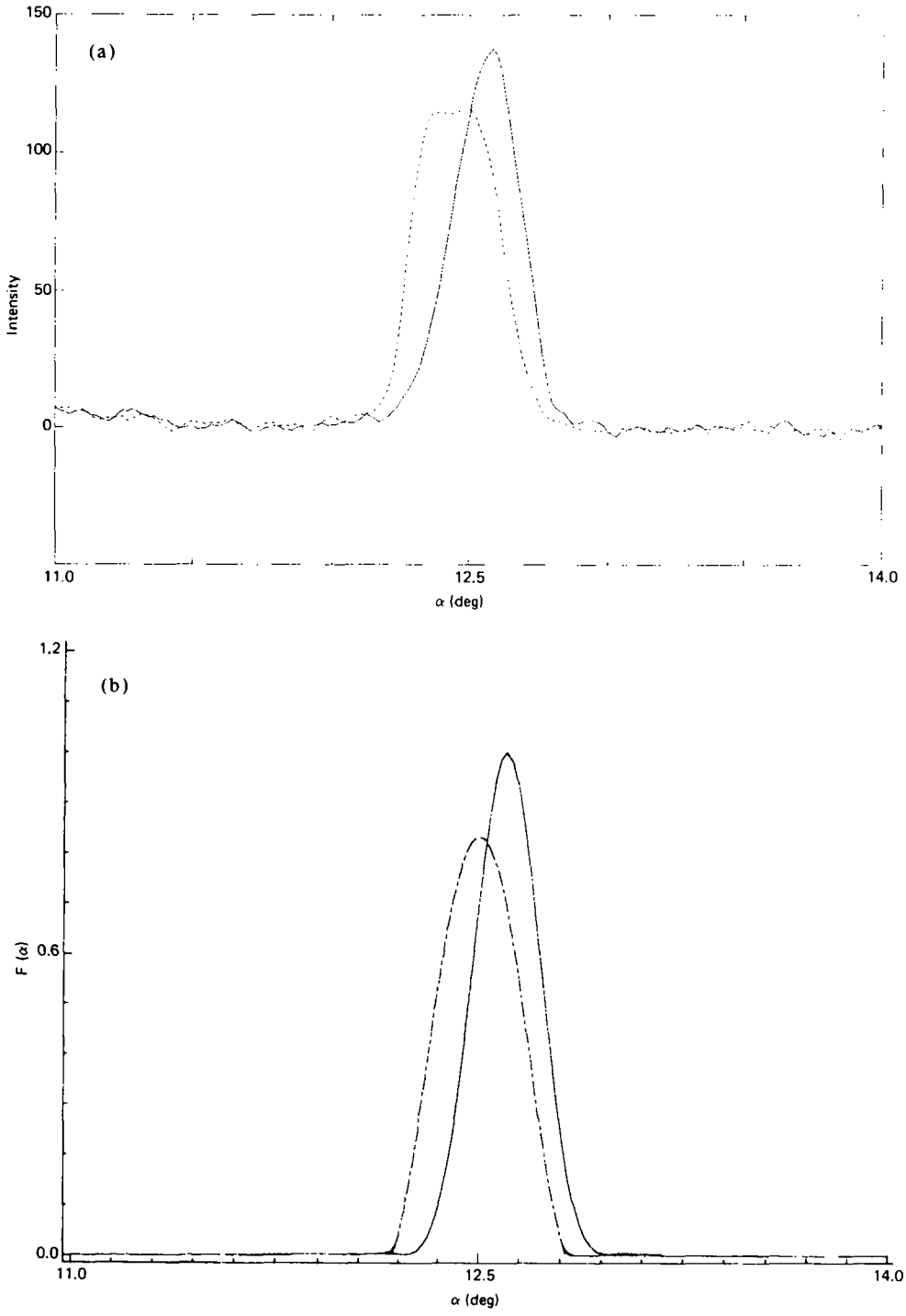

Fig. 5. (a) Experimental and (b) theoretical output (dashed lines) with respect to the inputs (solid lines) showing the shift due to the self scattering effect. The fanning is minimized by taking a narrow beam and a low propagation angle. The gaussian input beam propagated at an angle of 12.5° with the c-axis. Its waist was 15 μm. All angles are taken inside the crystal and the intensities are given in arbitrary units.

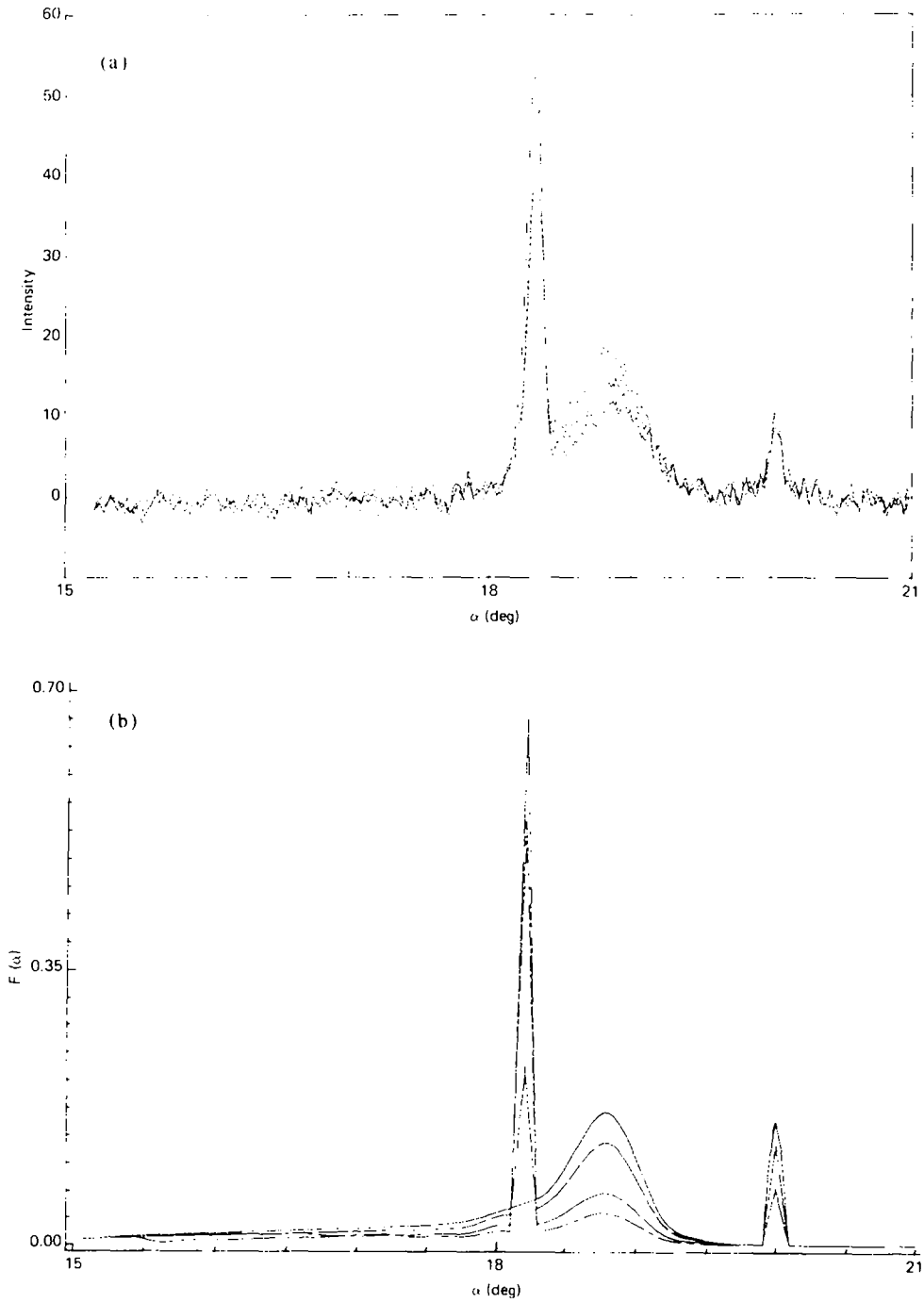

Fig. 6. Experimental (a) and theoretical (b) results showing the effect of a small signal with various input intensities (see text), which is amplified and depresses the fanning as the signal is increased (see values in the text). The strongest fanning corresponds to the case without signal. (The angles are taken inside the crystal.)

our calculations phase changes in the beam spatial frequency components. Linear phase changes due to the free propagation are negligible in short distances of few millimeters, and there is no contribution of nonlinear photorefractive phases in diffusion dominated wave mixing (see eq. (1) where γ_{ij} are real [6]).

We next study the effect of an additional signal beam on the fanning field. In fact, it is a study of the basic two-beam coupling process with the added unavoidable fanning. The usual purpose of such a configuration is signal amplification and oscillators [6]. Fig. 6 shows the experimental and theoretical outputs for three examples of input signal beams, having an angle of 18.3° and a relatively narrow spatial frequency width (expanded gaussian beam). The pump was a focused beam with waist of 12 μm and a spot size of 0.5 mm at the position of the crystal. In the experiment intensity ratios of the signal were $(14, 72, 380)\times10^{-5}$ with respect to the main beam (of about 10 mW), and in the calculation $(10, 50, 100)\times10^{-5}$. The reason for taking lower values in the calculation is that only a fraction of the input beam in the experiment is effectively involved in the mixing. We see that in all cases the signal is strongly amplified by two-beam coupling. The coupling constant of these discrete two beams (main and signal) is $\Gamma_{1,2}=8.44\ \mathrm{cm}^{-1}$. The process, however, is accompanied by a dramatic bleaching effect (or broad "hole burning") of the fanning (or the spatial frequency spectra), which is induced by the signal. We can see in fig. 6 the increasing depression of the fanning as the signal intensity is increased. At some point, the

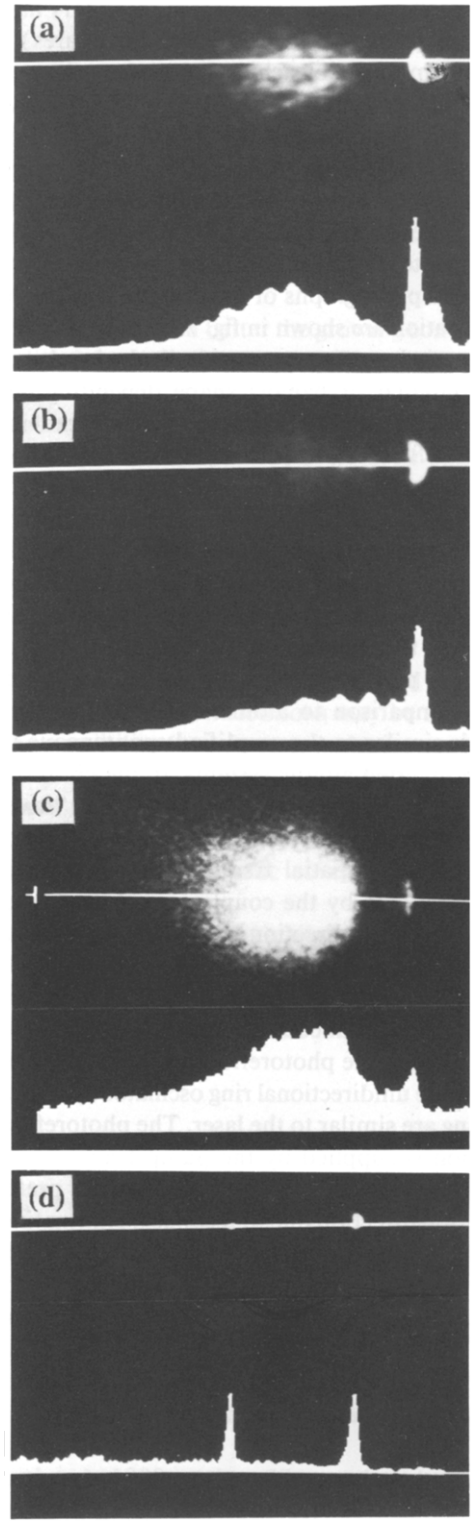

Fig. 7. Typical photographs of the fanning and signal amplification. The input cross section was circular (gaussian beam) in all experiments. The upper parts of the pictures give the output far field and the lower parts are the corresponding intensity plots along a horizontal line. (a) A picture of the fanning and the depletion of the main beam where the focus of the input beam was in front of the crystal. (b) The fanning and the depleted main beam for focusing the input behind the crystal. (c) When the depletion of the main beam is strong, a conical pattern of the main beam output was observed. (This is not seen in the experimental curves of the former graphs, in which the intensity was integrated over the vertical direction.) (d) The effect of a second signal beam which bleaches the fanning. For strong signals the fanning is almost completely eliminated and at some point a secondary fanning from the signal is built up (not shown here).

signal itself produces a significant secondary fanning structure (note shown in the present figures). The mechanism of the bleaching is based on the nonlinear strong coupling and the amplification which strongly favors the signal at the expense of noise amplification around it. A complete fanning suppression can be obtained where oscillation is built-up by the two-beam coupling (providing the unidirectional photorefractive oscillator [6]).

Typical photographs of the fanning and the signal amplification are shown in fig. 7. The output far field of the main beam is asymmetrically depleted and has a half circular or banana shape depending on the coupling degree. The depletion is observed in the right or left sides of the cross section depending on the position of the crystal with respect to the focus of the input beam. The photograph in fig. 7d shows the effect of a second signal, which bleaches the fanning.

The fanning, bleaching and "hole burning" effects, as well as the photorefractive oscillators and other aspects of photorefractive coupling, allow an interesting comparison to atomic systems. The fanning effect is similar to the amplified spontaneous emission in inverted atomic systems. In the photorefractive case the pump beam provides the "inverted state" of the photons which decay or scatter into other directions in a spatial frequency spectrum (directions), dictated by the coupling mechanism (given by eq. (3). Each direction is coherently amplified in the photorefractive medium. The bleaching of the fanning is similar to the situation in the frequency dependent spontaneous emission in atomic transitions. Finally, the photorefractive oscillators and especially the unidirectional ring oscillator by two-beam coupling are similar to the laser. The photorefractive inversion is supplied by the pump beam, of which photons are partially channeled into the preferred oscillation direction due to feedback, eliminating the fanning in other directions. It should be noted, however, that in the photorefractive case the temporal frequency spectrum of the fanning and oscillation are of basically different range than for lasers. Here we are talking about almost degenerate frequencies. The difference between the fanning or the oscillating beam and the pump frequencies is about $1-10^5$ Hertz. Another possible approach is to compare the fanning effect to stimulated scattering (Rayleigh, Raman etc.) and use the term of Stimulated Photorefractive Scattering as the suggestion in other works [8,9]. In fact, all of these processes have many common features.

In conclusion, we have conducted a study of photorefractive nonlinear multi two-wave mixing, which takes into account the full depletion of all waves. Our main purpose was the fanning effect and we have shown the importance of the amplified noise in producing it. The bleaching process of the fanning was also described and analyzed.

This work was supported by the Foundation for Research in Electronics, Computers and Communications, administrated by the Israel Academy of Science and Humanities and by the National Council for Research and Development, Israel, and the European Economic Community.

References

[1] B. Fischer and M. Segev, Appl. Phys. Lett. 54 (1989) 684.
[2] V.V. Voronov, I.R. Dorosh, Yu.S. Kuz'minov and N.V. Tkachenko, Sov. J. Quantum Electron. 10 (1981) 1346.
[3] J. Feinberg, J. Opt. Soc. Am. Vol. 72 (1982) 46.
[4] O.V. Kandidova, V.V. Lemanov and B.V. Sukharev, Sov. Phys. Solid State 28 (1986) 424.
[5] G. Zhang, Q.X. Li, P.P. Ho, Z.K. Wu and R.R. Alfano, Appl. Optics 25 (1986) 2955.
[6] B. Fischer, S. Sternklar and S. Weiss, IEEE J. Quantum Electron. QE-25 (1989) 550.
[7] M. Segev, Y. Ophir and B. Fischer, Appl. Phys. Lett., to be published.
[8] J.O. White, S.K. Kwong, M. Cronin-Golomb, B. Fischer and A. Yariv, Topics in Applied Physics Vol. 62 (Springer Verlag, 1989) p. 101.
[9] G.C. Valley, J. Opt. Soc. Am. B 4 (1987) 14.